

Voltage and dephasing probes: a full counting statistics discussion

Heidi Förster¹, Peter Samuelsson², Sebastian Pilgram³ and Markus Büttiker¹

¹ *Département de Physique Théorique, Université de Genève, CH-1211 Genève 4, Switzerland*

² *Department of Physics, University of Lund, Box 118, SE-22100, Sweden*

³ *Theoretische Physik, ETH Zürich, CH-8093 Zürich, Switzerland*

(Dated: October 28, 2018)

Voltage and dephasing probes introduce incoherent inelastic and incoherent quasi-elastic scattering into a coherent mesoscopic conductor. We discuss in detail the concepts of voltage and dephasing probes and develop a full counting statistics approach to investigate their effect on the transport statistics. The formalism is applied to several experimentally relevant examples. A comparison of different probe models and with procedures like phase averaging over an appropriate phase distribution shows that there is a perfect equivalence between the models for the case of one single-channel probe. Interestingly, the appropriate phase distribution is found to be uniform. A uniform distribution is provided by a chaotic cavity with a long dwell time. The dwell time of a chaotic cavity plays a role similar to the charge response time of a voltage or dephasing probe. For multi-channel or multiple probes the transport statistics of voltage and dephasing probes differs and the equivalence with phase averaging is similarly lost.

I. INTRODUCTION

In this work we are interested in the effect of voltage¹ or dephasing probes² on the transport statistics³ of mesoscopic few channel conductors. Voltage probes coupled to a coherent conductor permit incoherent *inelastic* processes: an electron entering the probe is thermalized by dissipation and later on fed back into the system. In contrast dephasing probes are *quasi-elastic* and non-dissipative, each electron exiting into the probe is reemitted within the same energy interval. Voltage probes can be used to describe a transition¹ from purely coherent transport to classical inelastic transport whereas dephasing probes can be used to describe a transition² from coherent transport to classical quasi-elastic transport.

The main motivation of this work is to provide an improved understanding of the physics of probe models. We achieve this by discussing the models on the level of full counting statistics (FCS) and by comparing them with each other and in addition with other procedures like phase averaging.⁴ The full counting statistics^{3,5} is characterized by a generating function from which conductance and noise and all current cumulants can be obtained simply by taking derivatives. For brief reviews on FCS see articles in Ref. 6.

Voltage and dephasing probe models are widely used, most often to address the disappearance of quantum effects in conductance. The transition from quantum combination of scatterer to the series addition of resistances is the subject of Ref. 1. Other applications include the role of equilibration of edge channel populations for the quantization of the Hall conductance⁷ and the transition from the quantum Hall effect to the classical Hall effect⁸, the role of dephasing in the quantum measurement process⁹ or the effect of inelastic processes in quantum pumping^{10,11}. The success of this approach is due to the fact that it can be directly incorporated in the formalism used to discuss the purely coherent limit. This is particularly evident in random matrix theory.^{12,13} Since

the scattering approach applies not only to conductance but also to noise and higher order current correlations, the role of inelastic scattering¹⁴ and dephasing¹⁵ in noise can also be investigated with this approach.

A brief account of our main results has been given in Ref. 4. We demonstrate that the generating function for an arbitrary conductor connected to only one single channel voltage probe agrees with the generating function of the conductor connected to a dephasing probe. A central result of our discussion is that the generating function of the one-channel probe models can also be obtained by phase averaging the generating function of the completely coherent conductor. Phase averaging is performed by connecting the conductor with the same strength as the voltage or dephasing probe to an external single mode scatterer characterized by a single phase with a given distribution⁴. Interestingly, the appropriate phase distribution which leads to a phase averaged result identical to that found from the voltage and dephasing probes is simply a uniform distribution. A mesoscopic scatterer which provides such a uniform distribu-

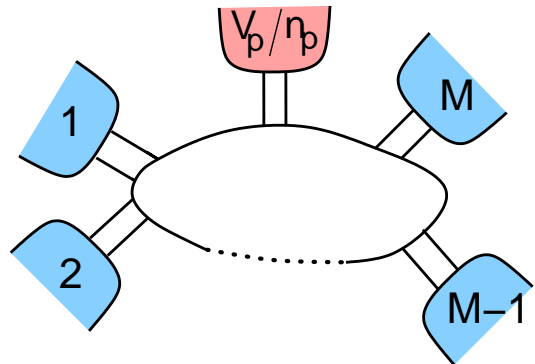


FIG. 1: (color online) A voltage (dephasing) probe described by the potential V_p (the occupation function n_p), connected to a mesoscopic conductor with M terminals.

tion is a chaotic cavity. A chaotic cavity, like a voltage or dephasing probe, reemits a carrier only with a certain time-delay. The importance of the time-delay is manifest even in the completely incoherent limit: then as we demonstrate⁴ at least for a particular geometry, the one-channel voltage or dephasing probe and phase averaging are equivalent to a classical exclusion statistics model¹⁶ provided the time-delay is also incorporated into the classical model.

The equivalence of voltage probe and dephasing probe models and phase averaging is a special property of one channel probes.⁴ Already for probes with more than one quantum channels it is known that the voltage probe model and the dephasing probe model give different results for conductance and noise.^{17,18} Furthermore a conductor connected to two (or more) voltage probes will in general exhibit a generating function that differs from the one obtained with two dephasing probes.⁴ We discuss in detail why there are differences between phase averaging and dephasing¹⁹ as soon as there are two or more probes.

We illustrate our basic results with the help of conceptually simple conducting structures. A prime example is the Mach-Zehnder interferometer: the simplicity here stems from the fact that there are no closed orbits. The electrical Mach-Zehnder interferometer was used to discuss dephasing in one-channel ballistic interferometers in Refs. 20,21,22,23. It has been experimentally realized in Ref. 24 and has since been the focus of a number of theoretical works^{25,26,27,28,29} followed by additional experiments^{30,31}. We mention that the recent experiment of Litvin et al.³¹ shows a visibility in conductance as a function of temperature and voltage which is in good agreement with theoretical results based on voltage probes²⁸.

Another conceptually simple setup which we will use to illustrate our results is a beam splitter structure^{32,33} coupled to dephasing and voltage probes^{17,18,34,35}. This example illustrates the dramatic difference between dephasing and voltage probes arising in the case of two transport channels: whereas in the presence of a dephasing probe current-current correlations remain negative, a voltage probe can generate positive current-current correlations^{17,18,35}, an effect demonstrated in a recent experiment by Oberholzer et al.³⁶. For a brief discussion of this and related experiments we refer the reader to Ref. 37.

In the presence of voltage and dephasing probes decoherence is a consequence of the escape of a carrier out of a coherence volume^{1,38}. This mechanism differs of course from other microscopic dephasing processes, such as electron-phonon or electron-electron scattering.³⁹ To the extent that voltage (or dephasing) probes are used to mimic the effect of these microscopic processes, they represent only a phenomenological description. However, voltage probes are of course real elements of mesoscopic conductors and the escape and reinsertion of carriers are true physical processes, if it is taken into account that the particles entering the probe are emitted not instan-

taneously but after a certain delay time. In this respect probe models are not phenomenological but provide an in principal fully quantum mechanical model which permits the investigation of decoherence in a scattering process that would in the absence of such probes be completely coherent. Indeed several authors have noticed and discussed the similarities between the description of inelastic processes on the level of quantum kinetic equations^{40,41} and the physics of voltage and dephasing probes.

Essentially voltage and dephasing probe models are an extension of a coherent scattering problem in which in addition to the true current and voltage terminals one considers a set of voltage or dephasing probes (see Fig. 1). Reducing this enlarged scattering problem^{1,2} with a set of boundary conditions which assure that there is not charge accumulation in the probes, one obtains a conduction problem with only the true voltage and current contacts. This leads to a description of transport which incorporates phase breaking processes to the extent that carriers visit the additional probes. On the level of conductance and noise the reduction from the large coherent problem to the incoherent fewer contact problem is straight forward. The reduction is more challenging if we want to capture the entire transport statistics. We formulate a stochastic path integral approach^{4,42,43} for the full counting statistics which treats the escape and injection process for voltage and dephasing probes. This approach uses separation of timescales in an essential manner: the delay time of the probe has to be much larger than the inverse average attempt frequency of scattering wave packets.

The effect of dephasing on the transport statistics for entangled states was recently studied, both for a probe model with conservation of average current only⁴⁴ as well as for a related model with full current conservation⁴⁵. Attempts at models with dephasing stubs which do not generate additional noise has lead to stubs in the form of chaotic cavities with long delay times⁴⁶. We present a detailed discussion of these and other related works in section IX.

II. VOLTAGE AND DEPHASING PROBES

Voltage and dephasing probes are used to introduce inelastic or elastic incoherent scattering respectively into a quantum coherent system. An additional terminal - either a voltage or a dephasing probe- is connected to a coherent mesoscopic conductor, as shown in Fig. 1. Particles entering the probe are later incoherently reemitted into the conductor. Scattering via the probe, a particle thus loses its phase coherence and in the case of a voltage probe, it also changes its energy.

A voltage probe is a real, physical component used in many mesoscopic experiments^{47,48,49,50}. It consists of a large metallic contact attached to the mesoscopic conductor, see Fig. 2. The contact is left floating or is connected to a voltmeter, i.e. ideally there is no current

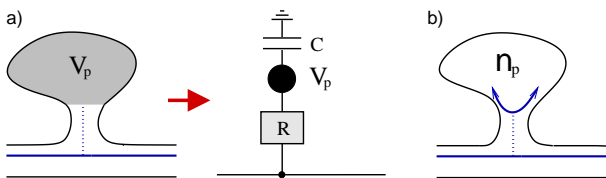


FIG. 2: (color online) (a) A voltage probe is a metallic contact with a floating potential V_p . It can be represented in an electrical circuit as a metallic region with capacitance C to the ground and charge relaxation resistance R . The low frequency current into the probe vanishes. (b) Model of a dephasing probe: the probe is described by a non-equilibrium occupation function n_p . The low frequency current vanishes separately in each energy interval.

drawn at the probe. In response to the injected charge on the probe, the potential $V_p = V_p(t)$ of the floating probe develops fluctuations on the timescale $\tau_d = RC$, as sketched in Fig. 3. Here R is the total charge relaxation resistance from the probe into the M terminals, where $1/R = \sum_{\alpha=1}^M G_{\alpha p}$ with $G_{\alpha p}$ the conductance from the probe to terminal α , and C is the total capacitance of the probe. The origin of these fluctuations has a very natural explanation: Injected charges raise the potential V_p which leads to an increase in the outgoing current. This consequently reduces the charge on the probe and with this V_p decreases etc. The timescale for the continuous charging and discharging of the probe is just as in classical circuit theory the RC -time. This picture clarifies, why current and current fluctuations at the probe at low frequencies $\omega < 1/\tau_d$ are completely conserved. Put differently, for a measurement during a time much longer than τ_d there is no charge accumulation in the probe.

We assume that the thermalization in the voltage probe is efficient, i.e. charges injected into the probe scatter inelastically on a timescale much shorter than τ_d . The electron occupation is thus described by an equilibrium Fermi-Dirac distribution $f_p(V_p, T)$. It is further assumed that the temperature T is fixed by the surrounding lattice, thus the voltage probe is dissipative and does not conserve heat current.

Contrary to the voltage probe, the dephasing probe is a

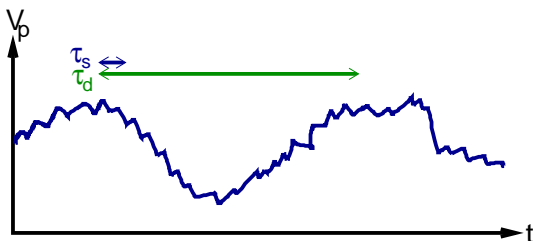


FIG. 3: (color online) Time-dependent potential $V_p(t)$ at a voltage probe. The current injected from the conductor into the probe gives rise to fast fluctuations on the time scale $\tau_s = h/eV$. The response of the probe gives rise to modulations on a much longer timescale $\tau_d = RC$.

conceptual tool used to model quasi-elastic dephasing². A particle injected in an energy interval E to $E + dE$ is incoherently emitted after spending an average time τ_d inside the probe, in the same energy interval. This allows an energy change of dE much smaller than the applied voltage eV or the temperature $k_B T$. The distribution function $n_p(E)$ in the energy interval is proportional to the number of carriers in the interval. As scattering in each energy interval is independent, $n_p(E)$ is -contrary to the distribution function of the voltage probe- a strongly non-equilibrium distribution function. Moreover, the fluctuations of the distribution function $n_p(E) = n_p(E, t)$ in each energy interval are independent. Their origin is qualitatively the same as those of the potential fluctuations in the voltage probe: the more charges injected into the probe, the larger is $n_p(E)$. This leads to an increase in the outgoing current and thus to a reduction of $n_p(E)$. The fluctuations of $n_p(E)$ occur on a timescale τ_d , the delay time of the probe. Again there is thus no charge accumulation of the probe on timescales longer than τ_d , and the current per energy into the probe is conserved up to the frequency $1/\tau_d$.

III. FULL COUNTING STATISTICS

We are interested in the full counting statistics, or the distribution of charges transmitted through the mesoscopic conductor in Fig. 1 during a measurement time τ . Let us first consider the conductor without the probe when only coherent elastic scattering is present. The distribution function is denoted by $P(\mathbf{Q})$ where the vector quantity $\mathbf{Q} = (Q_1, Q_2, \dots, Q_M)$ describes the charge transferred into each of the M terminals. $P(\mathbf{Q})$ can be expressed in terms of the cumulant generating function $S(\mathbf{\Lambda})$ by means of a Fourier transformation^{3,6}

$$P(\mathbf{Q}) = \int d\mathbf{\Lambda} e^{S(\mathbf{\Lambda}) - i\mathbf{\Lambda} \cdot \mathbf{Q}} \quad (1)$$

$$S(\mathbf{\Lambda}) = \ln \sum_{\mathbf{Q}} P(\mathbf{Q}) e^{i\mathbf{\Lambda} \cdot \mathbf{Q}}. \quad (2)$$

The vector $\mathbf{\Lambda} = (\lambda_1, \lambda_2, \dots, \lambda_M)$ contains the counting variables of the different terminals, the conjugate variables to \mathbf{Q} . The sum and integrals run over all elements of the vector, $\int d\mathbf{\Lambda} = (2\pi)^{-M} \int d\lambda_1 \dots d\lambda_M$ and $\sum_{\mathbf{Q}} = \sum_{Q_1 \dots Q_M}$. Probability conservation leads to the normalization of the generating function $S(\mathbf{0}) = 0$.

All irreducible moments are obtained by taking derivatives of the cumulant generating function with respect to the counting variables and evaluated at $\mathbf{\Lambda} = \mathbf{0}$. For a long measurement time τ the transmitted charge into a terminal α is proportional to τ , i.e. one can write $Q_\alpha = \tau I_\alpha$, and the zero frequency cumulants for the current can be expressed in terms of the generating function of the charge, Eq. (2). Written out explicitly, the first three

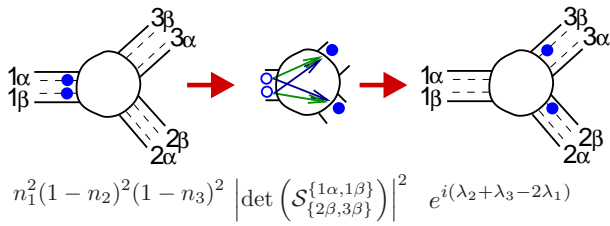


FIG. 4: (color online) A two-particle scattering event from channels 1α and 1β into 2β and 3β : the occupation probability is multiplied by the scattering probability and by the exponential factor containing the counting fields. The scattering probability $|\det(\mathcal{S}_{\{2\beta,3\beta\}}^{\{1\alpha,1\beta\}})|^2 = |\mathcal{S}_{2\beta,1\alpha}\mathcal{S}_{3\beta,1\beta} - \mathcal{S}_{2\beta,1\beta}\mathcal{S}_{3\beta,1\alpha}|^2$ represents the two indistinguishable processes shown above in the center, with the minus sign originating from the fermionic statistics of the particles.

cumulants are the average current

$$\langle I_\alpha \rangle = \frac{e}{i\tau} \frac{dS}{d\lambda_\alpha}, \quad (3)$$

the auto- or cross-correlations

$$C_{\alpha\beta} = \frac{e^2}{i^2\tau} \frac{d^2S}{d\lambda_\alpha d\lambda_\beta}, \quad (4)$$

and the skewness

$$C_{\alpha\beta\gamma} = \frac{e^3}{i^3\tau} \frac{d^3S}{d\lambda_\alpha d\lambda_\beta d\lambda_\gamma}. \quad (5)$$

For a general mesoscopic conductor described by a scattering matrix \mathcal{S} , Levitov and Lesovik⁵ derived an expression for the generating function S_0 (where the index 0 stands for a coherent system):

$$S_0 = \frac{1}{h} \int_0^\tau dt \int dE H_0 \text{ with} \quad (6)$$

$$H_0 = \ln \det \left[1 + \tilde{n} \left(\tilde{\lambda}^\dagger \mathcal{S}^\dagger \tilde{\lambda} \mathcal{S} - 1 \right) \right]. \quad (7)$$

For a conductor with single mode contacts to the M terminals, the scattering matrix has the dimensions $M \times M$. The matrix \tilde{n} contains the occupation numbers of the different terminals with $\tilde{n} = \text{diag}(n_1, n_2, \dots, n_M)$, and the matrix $\tilde{\lambda}$ introduces the counting fields, $\tilde{\lambda} = \text{diag}(e^{i\lambda_1}, e^{i\lambda_2}, \dots, e^{i\lambda_M})$. The generalization to many modes is straightforward: the dimension of all matrices in Eq. (7) grows according to the number of transport channels, but importantly all channels in the same terminal have the same occupation function and counting fields.

Probabilistic interpretation

In what follows we will frequently use the interpretation of the generating function in terms of multi-particle

scattering probabilities. The argument of the logarithm in Eq. (7) contains the probabilities of all scattering processes, each multiplied by an exponential factor containing counting variables that indicate the number and direction of transferred charges.

Technically the multi-particle probabilities are obtained by the expansion of the determinant⁵

$$\det \left[1 + \tilde{n} \left(\tilde{\lambda}^\dagger \mathcal{S}^\dagger \tilde{\lambda} \mathcal{S} - 1 \right) \right] = \sum_{\{a\}, \{b\}} \left| \det \left(\mathcal{S}_{\{b\}}^{\{a\}} \right) \right|^2 \times \prod_{i \in \{a\}} n_i \prod_{i \notin \{a\}} (1 - n_i) \exp \left(i \sum_{k \in \{b\}} \lambda_k - i \sum_{l \in \{a\}} \lambda_l \right) \quad (8)$$

Here $\{a\}$ denotes a set of transport modes -in general situated in different terminals-, from which particles are injected, and $\{b\}$ is the set of modes into which particles are transmitted. Because of particle conservation, the number of elements in set $\{a\}$ is in each particular scattering event equal to the number of elements in set $\{b\}$. The first sum in Eq. (8) runs over all possible sets $\{a\}$ and $\{b\}$, and represents all possible, distinct ways of scattering a number m of particles, with m ranging from 0 to the total number of transport modes in the M terminals. The probability that m particles are scattered from $\{a\}$ to $\{b\}$ is given by $|\det(\mathcal{S}_{\{b\}}^{\{a\}})|^2$, where the matrix $\mathcal{S}_{\{b\}}^{\{a\}}$ is formed by taking the intersecting matrix elements of the columns corresponding to the elements in $\{a\}$ and the rows corresponding to the elements in $\{b\}$ from the scattering matrix \mathcal{S} . The determinant expression originates from the indistinguishability of particles and their fermionic statistics: all possible transmission processes which convert an initial state of m particles in set $\{a\}$ into the final state of m particles in $\{b\}$ are obtained by exchanging successively pairs of the involved fermions. An explicit example of a two-particle process is shown in Fig. 4.

The products over the occupation functions of the different terminals in Eq. (8) determine the probability that exactly the m particles from set $\{a\}$ are injected. The exponent contains the sum of all counting fields of the emission channels of set $\{b\}$, and the corresponding sum of the injection channels of set $\{a\}$, multiplied by (-1) . This exponential factor works as a marker, indicating the direction and the number of transferred particles in a particular scattering event from $\{a\}$ to $\{b\}$ (compare also Fig. 4).

It turns out that in the expression of the expansion (8) independent processes factorize out, while alternative processes are added. This explains the integral over energy in the generating function $S_0 = \frac{1}{h} \int_0^\tau dt \int dE H_0$: in the long time limit all scattering events at different energies are independent, thus the expansion of the determinant -extended in energy- leads to a product, where each factor has the same form but stands for a different energy. This can be converted into an integral over the function H_0 .

IV. MACH-ZEHNDER INTERFEROMETER

To illustrate the full counting statistics and the probabilistic interpretation, we first discuss the Mach-Zehnder interferometer (MZI) without a probe. A scheme of the electronic MZI is shown in Fig. 5. It consists of two arms connected to four electronic reservoirs 1 to 4 via beam splitters A and B . The transmission (reflection) probability of the beam splitters is T_A and T_B (R_A and R_B) respectively. Transport in the single mode arms is unidirectional, corresponding to transport along edge-states in the quantum Hall regime. Such a setup was recently realized experimentally^{24,30,31}. Interference occurs, because the electrons have two alternative paths to propagate through the interferometer between beam splitter A and B . An Aharonov-Bohm flux Φ_{AB} threads the two arms, and the different vector potentials in the two arms lead to a phase difference $\Phi = \frac{2\pi e}{hc}\Phi_{AB}$. This difference creates a characteristic flux-periodicity in the interference pattern, the Aharonov-Bohm effect.

The conceptual simplicity of the interferometer originates from the exclusion of backscattering which discards closed orbits. As a consequence only the elements in the off-diagonal 2×2 blocks of the total 4×4 scattering matrix \mathcal{S} are non-vanishing²⁰. For our purposes we only need the processes from terminals 1 and 2 towards terminals 3 and 4 given in the lower off-diagonal block

$$\begin{aligned} \mathcal{S}_{31} &= -R_A R_B e^{i\Phi} + T_A T_B \\ \mathcal{S}_{42} &= T_A T_B e^{i\Phi} - R_A R_B \\ \mathcal{S}_{32} &= i\sqrt{R_A T_B} + i\sqrt{T_A R_B} e^{i\Phi} \\ \mathcal{S}_{41} &= i\sqrt{R_A T_B} e^{i\Phi} + i\sqrt{T_A R_B}. \end{aligned} \quad (9)$$

We consider equal length of the arms, giving energy-independent scattering amplitudes. Constant scattering phases can be absorbed into Φ . The second off-diagonal block describes independent processes from terminals 3 and 4 to 1 and 2 which are not indicated in Fig. 5 and which we do not need to specify here.

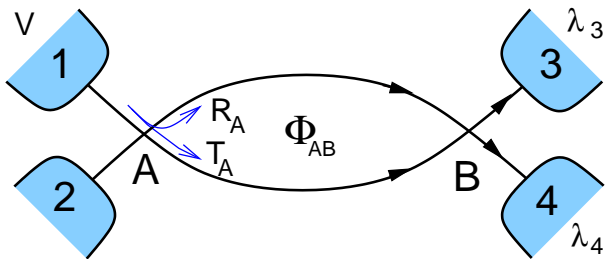


FIG. 5: (color online) Mach-Zehnder interferometer: a four-terminal conductor with unidirectional transport channels (indicated by arrows), threaded by a magnetic flux Φ_{AB} .

The generating function H_0 is obtained from Eq. (8):

$$\begin{aligned} H_0 &= \ln \left[((1 - n_1)(1 - n_2) \right. \\ &\quad + n_1(1 - n_2)(T_{31}e^{i(\lambda_3 - \lambda_1)} + T_{41}e^{i(\lambda_4 - \lambda_1)}) \\ &\quad + n_2(1 - n_1)(T_{32}e^{i(\lambda_3 - \lambda_2)} + T_{42}e^{i(\lambda_4 - \lambda_2)}) \\ &\quad \left. + n_1 n_2 e^{i(\lambda_4 + \lambda_3 - \lambda_2 - \lambda_1)} \right), \end{aligned} \quad (10)$$

where $T_{\alpha\beta} = |\mathcal{S}_{\alpha\beta}|^2$. Using the probabilistic interpretation, we can identify the different contributions: The term in the first line stands for the case that no particles are injected from terminals 1 or 2. The second and third line describe one-particle scattering from terminal 1 or 2 into either 3 or 4. The transmission probability of each process is multiplied by the counting factor, for example $T_{31}e^{i(\lambda_3 - \lambda_1)}$ marks a transfer from 1 to 3. The fourth line represents two infalling particles from 1 and 2, which end up in 3 and 4 via an exchange process: the events $1 \rightarrow 3$, $2 \rightarrow 4$ and $1 \rightarrow 4$, $2 \rightarrow 3$ are indistinguishable. Its probability is given by $|\det(\mathcal{S}_{\{3,4\}}^{\{1,2\}})|^2 = |\mathcal{S}_{31}\mathcal{S}_{42} - \mathcal{S}_{32}\mathcal{S}_{41}|^2$ which is here equal to one as a consequence of the Pauli principle.

In the simplest case of zero temperature, and a voltage applied at terminal 1, the electron occupation function is unity in reservoir 1 and zero in reservoirs 2 – 4 in the energy interval $0 \leq E \leq eV$. Then all charges are incident from contact 1, and only one-particle processes take place. Each infalling particle has exactly two final states, characterized by transmission into either contact 3 or 4. Therefore, the interferometer acts like a beam splitter and the statistics of transmitted charge is a binomial distribution. The cumulant generating function is obtained from Eq. (10) as

$$S_0 = N \ln [T_{31}e^{i(\lambda_3 - \lambda_1)} + T_{41}e^{i(\lambda_4 - \lambda_1)}], \quad (11)$$

where $N = \frac{eV\tau}{h}$ can be understood as the number of infalling wave packets during the measurement time τ . Probability conservation requires $T_{31} + T_{41} = 1$. Because of charge conservation, the generating function depends only on the differences $\lambda_3 - \lambda_1$ and $\lambda_4 - \lambda_1$. In order to obtain all information about the transmitted charge it is sufficient to count the number of particles in one of the contacts 3 or 4. Here, we set $\lambda_1 = \lambda_4 = 0$ and perform the Fourier transform with respect to λ_3 . We obtain the distribution function $P(Q_3) = \binom{N}{Q_3} T_{31}^{Q_3} (1 - T_{31})^{N - Q_3}$ for the charge Q_3 transmitted into contact 3, a binomial distribution. Note that the transmission probability $T_{31} = R_A R_B + T_A T_B - 2\sqrt{R_A R_B T_A T_B} \cos \Phi$ depends on the magnetic flux, and the correlations between the current in 3 and 4, $C_{34} = -\frac{e^3 V}{h} T_{31} (1 - T_{31})$, are negative as is generally the case for mesoscopic structures in a zero impedance external circuit⁵¹.

Probe coupled to the interferometer

We want to address the question of how the distribution of transmitted charges is affected by coupling the MZI to a voltage or dephasing probe? After adding the additional terminal as shown in Fig. 6 the setup is described by a 5×5 scattering matrix. In the case above of zero temperature and a voltage applied only to terminal 1, the occupation functions of terminals 1–4 are known but the occupation of the probe n_p is not determined. While in the coherent interferometer only one-particle processes with two possible final states were allowed, the additional probe opens up additional paths and leads to two-particle processes. It is instructive to group the different contributions to H_0 into scattering processes according to the number of particles entering or leaving the probe. This gives

$$\begin{aligned}
 H_0 = & \ln \left[(1 - n_p) \left((R_A R_B (1 - \varepsilon) + T_A T_B) e^{i\lambda_3} \right. \right. \\
 & + (R_A T_B (1 - \varepsilon) + T_A R_B) e^{i\lambda_4} \\
 & \left. \left. + 2\sqrt{R_A T_A R_B T_B (1 - \varepsilon)} \cos \Phi (e^{i\lambda_4} - e^{i\lambda_3}) \right) \right. \\
 & + n_p \left((R_A R_B + T_A T_B (1 - \varepsilon)) e^{i\lambda_3} \right. \\
 & + (R_A T_B + T_A R_B (1 - \varepsilon)) e^{i\lambda_4} \\
 & \left. \left. + 2\sqrt{R_A T_A R_B T_B (1 - \varepsilon)} \cos \Phi (e^{i\lambda_4} - e^{i\lambda_3}) \right) \right. \\
 & \left. + n_p \varepsilon T_A e^{i(\lambda_3 + \lambda_4 - \lambda_p)} + (1 - n_p) \varepsilon R_A e^{i\lambda_p} \right]. \quad (12)
 \end{aligned}$$

The different processes are illustrated in Fig. (7) and consist of i) no charge moving into or out of the probe (the first three lines in Eq. (12), multiplied by $(1 - n_p)$), ii) processes where one particle is entering and one is leaving the probe (line 4 to 6, multiplied by n_p), iii) processes where one particle is leaving the probe (the first term in the last line) and iv) one particle is entering it (the very last term in Eq. (12)).

As discussed in section II, a defining property of the probe is charge conservation on timescales longer than the delay time τ_d of the probe. This means that all cumulants of the current flowing into the probe are zero for low frequencies $\omega \ll 1/\tau_d$. Clearly, the expression for

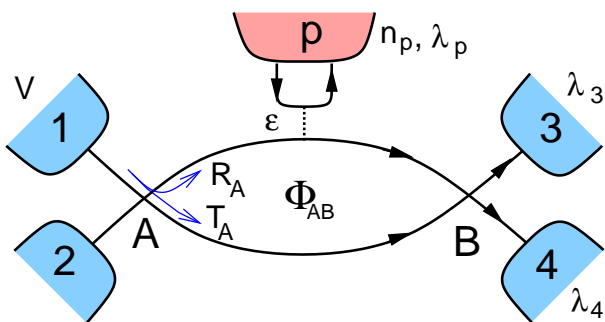


FIG. 6: (color online) The upper arm of the Mach-Zehnder interferometer is coupled to a dephasing or voltage probe with coupling strength ε .

the generating function, Eq. (12) is then not the solution, since current and current fluctuations at the dephasing probe obtained from derivatives with respect to λ_p are non-zero. Also the occupation n_p (and λ_p) is fluctuating, which is not taken into account in Eq. (12). Therefore, this equation is defining an unconstrained generating function: it treats the dephasing probe like any other charge absorbing terminal. The question is now, what is the correct expression for the FCS for a dephasing or a voltage probe attached to the conductor?

V. STOCHASTIC PATH INTEGRAL

To arrive at the correct answer we make use of the stochastic path integral (SPI) technique developed in Refs. 42,43. The stochastic path integral approach is one of a number of techniques which can be used to find the generating function^{6,52}. The cornerstone of the stochastic path integral technique is the separation of timescales. In mesoscopic systems the current typically exhibits fluctuations with two qualitatively different physical origins: i) the intrinsic current fluctuations, resulting from probabilistic scattering of individual charges, which occur on a timescale of the order τ_s , and ii) the fluctuations of potentials or distribution functions arising as a current conserving response to the intrinsic fluctuations, which occur on a timescale of the order τ_d , the dwell or delay time (compare also Fig. 3).

For our system, a general mesoscopic scatterer connected to a voltage or a dephasing probe (see Fig. 1), the short timescale is given by the average distance in time between two successive wave packets, typically of the order of $\tau_s = h/eV$. The long timescale is given by the delay time of the probe τ_d . It is thus essential for the application of the SPI that

$$\tau_s \ll \tau_d \quad (13)$$

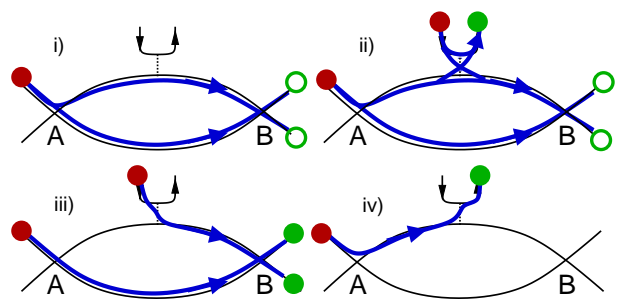


FIG. 7: (color online) i) No particles are moving in or out of the probe. ii) One particle enters, one leaves the probe, thus there is no net charge transfer into the probe. iii) One particle is emitted from the probe. iv) One particle enters the probe. i) and iv) are one-particle processes, and ii) and iii) two-particle processes. Note full red dots represent injected particles and filled (empty) green circles represent the one (two) final states.

or in other words that the applied voltage is large enough $eV \gg \hbar/\tau_d$.

Based on the separation of timescales, we introduce for the derivation of the SPI an intermediate time step Δt with $\tau_s \ll \Delta t \ll \tau_d$, during which the charge in the probe (and its counting variable λ_p) changes marginally. The FCS for this time interval is given by the Levitov-Lesovik formula Eq. (6) for a scatterer connected to the probe, i.e. the unconstrained generating function. The charge fluctuations in two successive time intervals Δt can be expressed in terms of the distribution functions of charge transferred during each of the two time intervals. By stepwise extending this result to longer times and taking the continuum limit, we finally obtain the distribution function $P(\mathbf{Q})$ in terms of a stochastic path integral. A formal derivation of the SPI is given in the appendix A, here we simply state the results, first for the dephasing probe and thereafter for the voltage probe.

A. Dephasing probe

In the dephasing probe, the low frequency currents per energy interval into the probe are conserved due to fluctuations of the occupation number $n_p(E, t)$. For a coherent conductor to which a dephasing probe is connected, the generating function S in Eq. (2) is obtained by the stochastic path integral over all possible distribution functions n_p and values of the counting variable λ_p at the dephasing probe,

$$\exp(S) = \int \mathcal{D}n_p \mathcal{D}\lambda_p \exp(\tilde{S}), \quad (14)$$

where

$$\tilde{S} = \frac{1}{\hbar} \int_0^\tau dt \int dE [-i\tau_d \lambda_p \dot{n}_p + H_0]. \quad (15)$$

Thus the additional term $-i\tau_d \lambda_p \dot{n}_p$ in Eq. (15) takes into account charge conservation on the probe.

In general the path integral in n_p and λ_p can not be evaluated exactly. It is however possible to evaluate the integral in saddle point approximation. The underlying idea of the saddle point approximation is that the main contribution to the integral comes from the region around the stationary, or saddle point, where

$$\frac{\delta \tilde{S}}{\delta n_p} = 0, \quad \frac{\delta \tilde{S}}{\delta \lambda_p} = 0. \quad (16)$$

Note that here both n_p and λ_p depend on both energy and time. Away from the saddle point the integrand fluctuates rapidly as a function of n_p and λ_p , giving a small contribution to the integral. We thus expand \tilde{S} to second order around the saddle point as

$$\tilde{S} = \tilde{S}^0 + \frac{1}{2} \Delta \lambda_p^2 \frac{\delta^2 \tilde{S}}{\delta \lambda_p^2} + \frac{1}{2} \Delta n_p^2 \frac{\delta^2 \tilde{S}}{\delta n_p^2} + \Delta \lambda_p \Delta n_p \frac{\delta^2 \tilde{S}}{\delta \lambda_p \delta n_p} \quad (17)$$

Here $\Delta \lambda_p = \lambda_p - \lambda_p^0$ and $\Delta n_p = n_p - n_p^0$ where λ_p^0 and n_p^0 are solutions to the saddle point equations (16). The zeroth order solution \tilde{S}^0 is just \tilde{S} with the saddle point solutions λ_p^0 and n_p^0 inserted. As is shown in the appendix B, the Gaussian fluctuations around the saddle point only give rise to corrections of the order $\tau_s/\tau_d \ll 1$. This means that as long as the underlying condition for the SPI, Eq. (13) is fulfilled, the saddle point approximation $S = \tilde{S}^0$ is a good one.

Carrying out the functional derivatives $\delta \tilde{S}/\delta n_p$ and $\delta \tilde{S}/\delta \lambda_p = 0$ we arrive at the saddle point equations for λ_p and n_p

$$i\dot{n}_p = \frac{1}{\tau_d} \frac{\partial H_0}{\partial \lambda_p}, \quad i\dot{\lambda}_p = -\frac{1}{\tau_d} \frac{\partial H_0}{\partial n_p}. \quad (18)$$

In this paper we will only consider the stationary limit, $\tau \gg \tau_d$. In this limit the time derivatives $\dot{\lambda}_p$ and \dot{n}_p can be neglected, the functional integrals are reduced to normal integrals and the function $\tilde{S} \equiv \bar{S}$ becomes proportional to the measurement time

$$\bar{S} = \frac{\tau}{\hbar} \int dE H_0 \quad (19)$$

Consequently, the saddle point equations are reduced to

$$\frac{\partial H_0}{\partial \lambda_p} = 0, \quad \frac{\partial H_0}{\partial n_p} = 0. \quad (20)$$

In the general case, with many transport modes in the contacts between the probe and the conductor, the saddle point equations are highly nonlinear in both λ_p and n_p and it is only possible to solve them numerically. In the case with a single mode the solution can be found analytically. Just as for the special case of the MZI discussed above (see Fig. 7), all possible scattering processes belong to one of the four different groups: i) no particle injected into and no particle emitted from the probe, ii) one particle injected into and one emitted from the probe, iii) no particle injected but one emitted and iv) one particle injected into but none emitted. Due to the Pauli principle no other processes exist, i.e. it is not possible for more than one particle to leave or enter the single mode probe in the same scattering process. Making use of the expansion of the generating function in terms of multi-particle scattering probabilities, Eq. (8), we can write the generating function as

$$H_0(n_p, \lambda_p) = \ln [(1 - n_p) (q_{00} + q_{01} e^{i\lambda_p}) + n_p (q_{11} + q_{10} e^{-i\lambda_p})] \quad (21)$$

Here we introduced the notation q_{kl} for the total multiple scattering probabilities (multiplied with the appropriate counting field expressions). The index $l = 0, 1$ denotes the number of particles injected into the probe, and $k = 0, 1$ the number of particles emitted from the probe. It is possible to express q_{kl} in a compact form in terms of a

number of determinants F_{kl} , defined as

$$\begin{aligned} F_{kl} &= \det[1 + \bar{n}_k(\bar{\lambda}_1^\dagger \mathcal{S}^\dagger \bar{\lambda}_l \mathcal{S} - 1)] \\ \bar{n}_k &= \text{diag}(n_1, n_2, \dots, n_M, k) \\ \bar{\lambda}_k &= \text{diag}(e^{i\lambda_1}, e^{i\lambda_2}, \dots, e^{i\lambda_M}, k). \end{aligned} \quad (22)$$

Here, \bar{n}_k and $\bar{\lambda}_k$ are diagonal matrices of the distribution functions and counting fields respectively, with the last entry, corresponding to the probe terminal, just given by the number $k = 0, 1$. The relation between q_{kl} and F_{kl} is given by

$$\begin{aligned} q_{00} &= F_{00}, & q_{01} &= F_{01} - F_{00}, \\ q_{10} &= F_{10}, & q_{11} &= F_{11} - F_{10}. \end{aligned} \quad (23)$$

For H_0 in Eq. (21), the second saddle point equation in (20) gives

$$\frac{\partial H_0}{\partial n_p} = - (q_{00} + q_{01}e^{i\lambda_p}) + q_{11} + q_{10}e^{-i\lambda_p} = 0 \quad (24)$$

from which one obtains the expression for λ_p^0

$$e^{i\lambda_p^0} = \frac{q_{11} - q_{00} + \sqrt{(q_{11} - q_{00})^2 + 4q_{01}q_{10}}}{2q_{01}} \quad (25)$$

The correct sign in this solution is defined by the normalization $H_0(\mathbf{\Lambda} = 0) = 0$. Inserting this back into the generating function, noting the terms proportional to n_p drop out, we get the generating function

$$S = N \ln \left[\frac{1}{2} \left(\mathcal{A} + \sqrt{\mathcal{A}^2 - 4\mathcal{B}} \right) \right] \quad (26)$$

with $\mathcal{A} = q_{00} + q_{11} = F_{00} + F_{11} - F_{10}$ and $\mathcal{B} = q_{00}q_{11} - q_{01}q_{10} = F_{00}F_{11} - F_{01}F_{10}$ and $N = eV\tau/h$. This is the general expression of the *constraint generating function* for a conductor coupled to a single mode dephasing probe. The interpretation of this function is not as straightforward as the probabilistic expansion of the unconstraint function H_0 , Eqs. (7) and (8). Both the parameters \mathcal{A} and \mathcal{B} contain multi-particle scattering processes, but \mathcal{A} represents only processes without any net charge transfer into the probe. The square root term technically originates from the fact that the saddle point equation Eq. (24) is quadratic in $e^{i\lambda_p}$, which reflects that in one scattering event, the charge in the probe can be increased or diminished by one.

B. Voltage probe

In the voltage probe, the potential V_p fluctuates in response to the injected current fluctuations. Just as for the dephasing probe the potential fluctuations lead to current conservation on the timescale of τ_d . For the voltage probe it is however the total energy integrated current that is conserved. The effect of the fluctuating voltage on the FCS can again be incorporated via the

stochastic path integral over the potential V_p and the energy independent counting variable λ_p as

$$\exp(S_V) = \int \mathcal{D}V_p \mathcal{D}\lambda_p \exp(\tilde{S}_V), \quad (27)$$

where

$$\tilde{S}_V = \frac{1}{h} \int_0^\tau dt \left[-i\tau_d \lambda_p e \dot{V}_p + \int dEH_0 \right]. \quad (28)$$

In the long measurement time limit $\tau \gg \tau_d$ the time derivatives can be neglected and we have, analogous to Eq. (19)

$$\bar{S}_V = \frac{\tau}{h} \int dEH_0, \quad (29)$$

where we note that V_p enters in the distribution function n_p of the probe. The saddle point equations are

$$\frac{\partial \bar{S}_V}{\partial \lambda_p} = 0, \quad \frac{\partial \bar{S}_V}{\partial V_p} = 0. \quad (30)$$

Focusing on the zero temperature limit and on energy independent scattering only, we can write the function

$$\begin{aligned} \bar{S}_V &= \frac{\tau}{h} \left[\int_0^{eV_p} dEH_0|_{n_p=1} + \int_{eV_p}^{eV} dEH_0|_{n_p=0} \right] = \\ &= \frac{e\tau}{h} (V_p H_0|_{n_p=1} + (V - V_p) H_0|_{n_p=0}). \end{aligned} \quad (31)$$

This function is linear in the applied voltage V and in the potential of the probe V_p even for many transport channels. The second saddle point equation in Eq. (30), makes the part proportional to V_p drop out and at the same time determines the saddle point solution for the counting field λ_p^0 . For the constraint generating function we obtain⁴

$$S_V = \frac{eV\tau}{h} H_0|_{n_p=1, \lambda_p^0}. \quad (32)$$

For a single transport mode the solution to the second saddle point equation, Eq. (30), is identical to the one for the dephasing probe and we arrive again at the expression in Eq. (25). The generating function S_V is consequently identical to Eq. (26), $S_V = S$. There is thus *no difference* between a dephasing and a voltage probe for the case of a single mode probe and energy independent scattering. However, if there are more than one single mode probe, multi-mode probes or energy dependent scattering, the different electron occupation in the voltage and dephasing probes lead to different transport statistics. This is explained in section VIII for an example of a conductor with two transport channels coupled to either a voltage or a dephasing probe.

VI. THE MACH-ZEHNDER INTERFEROMETER WITH THE PROBE

The coherent Mach-Zehnder interferometer at zero temperature and with a voltage V applied at terminal 1 is characterized by a binomial distribution, as explained in detail in section IV. We first note that the cumulant generating function S_0 , Eq. (11), can be rewritten as

$$S_0 = N \ln[b + c \cos \Phi]. \quad (33)$$

Here, the different terms in the transmission probabilities T_{31} and T_{41} are rearranged into the parameter b and c . The parameter $b = (T_A T_B + R_A R_B)e^{i\lambda_3} + (T_A R_B + R_A T_B)e^{i\lambda_4}$ represents the classical contribution due to particles which go either along the upper or the lower arm, and $c \cos \Phi$ stands for the coherent quantum interference contribution with $c = 2\sqrt{R_A T_A R_B T_B}(e^{i\lambda_4} - e^{i\lambda_3})$. The counting variable λ_1 is set to zero.

Fig. 6 shows the MZI with a dephasing probe connected to the upper arm. The full counting statistics for the interferometer with the probe attached is obtained by applying the formalism of section V A. Solving the saddle point equations in Eq. (20) with H_0 given by Eq. (12) we find for the constraint cumulant generating function

$$S = N \ln \left[b \left(1 - \frac{\varepsilon}{2} \right) + c \sqrt{1 - \varepsilon} \cos \Phi + \frac{\varepsilon}{2} \sqrt{b^2 - c^2} \right]. \quad (34)$$

In comparison to the result for the coherent interferometer, Eq. (33), the interfering contribution is attenuated by the factor $\sqrt{1 - \varepsilon}$. Thus, as expected the generating function becomes flux independent in the limit of strong dephasing

$$S_{\varepsilon=1} = N \ln \left[\frac{b}{2} + \frac{1}{2} \sqrt{b^2 - c^2} \right]. \quad (35)$$

In addition, the parameter b is in Eq. (34) multiplied by a reduction factor $(1 - \varepsilon/2)$, and a third contribution $\varepsilon \sqrt{b^2 - c^2}/2$ appears. As pointed out in section IV, the processes into and out of the probe give rise to exchange, or two-particle interference processes, for example $1 \rightarrow 3, p \rightarrow p$ and $1 \rightarrow p, p \rightarrow 3$, which are indistinguishable. Note that the processes with particles moving along either of the arms (b) are reduced, regardless of the fact that the probe is coupled to the upper arm only.

The first two cumulants obtained from Eq. (34) reproduce known results for current and noise^{20,25,28}. For completeness we present the first three cumulants for the

case of equal beam splitters, $R_A = R_B = R = 1 - T$,

$$I_3 = \frac{e^2 V}{h} (R^2 + T^2 - 2RT \sqrt{1 - \varepsilon} \cos \Phi), \quad (36)$$

$$C_{33} = \frac{e^3 V}{h} 2RT \left[(R^2 - RT + T^2) + (R - T)^2 \sqrt{1 - \varepsilon} \cos \Phi - RT(1 - \varepsilon) \cos 2\Phi \right], \quad (37)$$

$$C_{333} = \frac{e^4 V}{h} 2RT \left[-(R - T)^2 (R^2 - 3RT + T^2) + (2R^2 T^2 - (R - T)^2 (R^2 - 6RT + T^2)) \sqrt{1 - \varepsilon} \cos \Phi + 3RT(R - T)^2 (1 - \varepsilon) \cos 2\Phi - 2R^2 T^2 (1 - \varepsilon)^{\frac{3}{2}} \cos 3\Phi \right]. \quad (38)$$

Each cumulant contains oscillating terms proportional to $\cos(\Phi), \cos(2\Phi), \dots, \cos(k\Phi)$, where k is the order of the cumulant. As is clear from Eqs. (36)-(38), the effect of coupling the MZI to the probe is to multiply the oscillating terms proportional to $\cos(k\Phi)$ with damping factors²⁸ $(1 - \varepsilon)^{k/2}$. Importantly, the Φ -independent terms in the cumulants are however not affected by the coupling to the probe. Despite the complicated multi-particle origin of the contributions to the generating function, Eq. (34), the only effect of the probe is thus to damp the AB-oscillations in the cumulants.

Similarly, a second single mode probe attached to the MZI with coupling strength ε' results only in modifying the damping factor of the oscillations in the cumulants in the following way: $(1 - \varepsilon)^{k/2} \rightarrow (1 - \varepsilon)^{k/2} (1 - \varepsilon')^{k/2}$. Again it does not matter if the additional probe is coupled to the same or the other interferometer arm.

For energy-independent scattering considered here, the discussion at the end of section V B applies and Eq. (34) does not change if the dephasing probe is exchanged with a single mode voltage probe. This is however not the case for more than one probe⁴.

VII. PHASE AVERAGING

The reduction of the oscillating terms in the cumulants due to the coupling of the MZI to a probe, indicates that the effect of a dephasing probe can be explained in terms of phase averaging^{25,28}. Consider the interferometer coupled with strength ε not to a dephasing probe, but to an additional elastic coherent scatterer ϕ as depicted in Fig. 8. Every particle incident on contact ϕ is returned coherently with a phase factor $e^{i\varphi}$. An electron in the upper arm of the interferometer can enter the contact ϕ and after multiple internal reflections continue on its path with an additional phase factor $e^{i\tilde{\varphi}}$. This additional phase factor enters into the coherent generating function as $H_0(\Phi) \rightarrow H_0(\Phi + \tilde{\varphi})$.

We make the simplest possible assumption that the phase φ is uniformly distributed between 0 and 2π . Then the electron phase $\tilde{\varphi}$ is related to the scattering phase by $\varphi = \tilde{\varphi} + \pi + 2 \arctan[\sqrt{1 - \varepsilon} \sin \tilde{\varphi} / (1 - \sqrt{1 - \varepsilon} \cos \tilde{\varphi})]$ and

obeys a periodic distribution function⁴

$$f(\tilde{\varphi}) = \frac{1}{2\pi} \frac{d\varphi}{d\tilde{\varphi}} = \frac{1}{2\pi} \frac{\varepsilon}{2 - \varepsilon + 2\sqrt{1 - \varepsilon} \cos(\tilde{\varphi})}. \quad (39)$$

The average of the coherent generating function for the MZI is with Eq. (33) given by

$$S = \langle S_0 \rangle_\varphi = N \int_0^{2\pi} d\tilde{\varphi} f(\tilde{\varphi}) H_0(\Phi + \tilde{\varphi}) \quad (40)$$

and agrees exactly with the result (34) obtained from the dephasing probe model.

Interestingly, it is possible to obtain such a phase average of the cumulant generating function by taking the additional elastic, coherent scatterer to be a single mode chaotic cavity with a long dwell time, equal to the delay time of the probe $\tau_d \gg h/eV$. The scattering phase φ picked up by electrons scattering at the cavity depends on energy. It is known from random matrix theory¹³ that scattering amplitudes at two different energies E and $E+dE$ are uncorrelated if the energy difference dE is much larger than the inverse dwell time h/τ_d . Put differently, an electron at energy E sees a completely different cavity scattering potential than an electron at $E+dE$. Since $eV \gg h/\tau_d$, the integral over energy of the cumulant generating function, Eq. (19), for the MZI connected to the cavity effectively means a sum over a large number of realizations of cavity scattering potentials, i.e. an ensemble average. It is also well known from random matrix theory¹² that the phase φ of an ensemble of single mode cavities is uniformly distributed between 0 and 2π . Formally, since the scattering in the MZI itself is independent on energy in the interval 0 to eV , we can thus write $\int_0^{eV} dE \rightarrow \frac{eV}{2\pi} \int_0^{2\pi} d\varphi$, and we arrive at the phase average of Eq. (40).

We note that from Eq. (40) it is clear why the dephasing probe model exclusively affects the oscillating contributions to the cumulants: the function H_0 can be

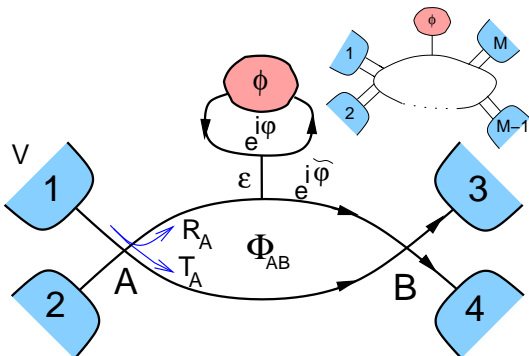


FIG. 8: (color online) Phase averaging: a particle enters the elastic scatterer ϕ with probability ε and obtains a uniformly distributed phase factor $e^{i\varphi}$. After multiple internal reflections it leaves the scatterer with an overall phase $e^{i\tilde{\varphi}}$. The inset shows a general conductor to which an elastic scatterer ϕ is connected.

expanded in terms of the cumulants, and the phase averaging leaves the contributions that are independent of Φ unchanged while it damps the oscillations.

General conductor

The correspondence between phase averaging and the dephasing/voltage probe model also holds for a general mesoscopic conductor with M terminals. Instead of a single mode (dephasing/voltage) probe, an elastic scatterer ϕ is via a single mode connection coupled to the conductor as shown in the inset of Fig. 8.

We define a $(M+1) \times (M+1)$ scattering matrix \mathcal{U} of the conductor with the additional contact ϕ that can be written in a block form

$$\mathcal{U} = \begin{pmatrix} \mathcal{S}_{00} & \mathcal{S}_{0\phi} \\ \mathcal{S}_{\phi 0} & \mathcal{S}_{\phi\phi} \end{pmatrix}. \quad (41)$$

Here the $M \times M$ block \mathcal{S}_{00} describes scattering between the M terminals of the conductor, the $M \times 1$ ($1 \times M$) block $\mathcal{S}_{\phi 0}$ ($\mathcal{S}_{0\phi}$) the scattering from (to) the conductor to (from) the phase contact ϕ and complex number $\mathcal{S}_{\phi\phi}$ the reflection from the contact ϕ back to ϕ . The total $M \times M$ scattering matrix \mathcal{S} for the conductor connected to the elastic scatterer ϕ can then be written as

$$\mathcal{S} = \mathcal{S}_{00} + \mathcal{S}_{0\phi} \frac{e^{i\varphi}}{1 - \mathcal{S}_{\phi\phi} e^{i\varphi}} \mathcal{S}_{\phi 0}. \quad (42)$$

Inserting this scattering matrix into Eq. (7), the generating function $H_0(\varphi)$ depends on φ . We then average the cumulant generating function $H_0(\varphi)$ over the uniformly distributed phase φ as

$$\langle H_0 \rangle_\varphi = \frac{1}{2\pi} \int_0^{2\pi} d\varphi H_0(\varphi). \quad (43)$$

We show in appendix D that the averaged generating function $\langle H_0 \rangle_\varphi$ is identical to the result for the dephasing (or voltage) probe, Eq. (26), valid for an arbitrary mesoscopic conductor connected to a single mode probe.

It is important to point out that for any geometry containing two or more single mode probes, the phase averaging approach does in general not give the same result as the dephasing probe model. The reason for this is that interference between scattering paths that pass the different probes/contacts p_j/ϕ_j in different order (but the same number of times) survives phase averaging but is suppressed by dephasing probes. A more detailed discussion of this together with concrete examples where the dephasing probe and phase averaging approaches give different results, are presented in appendix E. We also point out that for probes with more than one mode there is no obvious generalization of the phase averaging approach. An investigation in various models for phase averaging in multi-mode probes is beyond the scope of the present paper and thus deferred to a future publication.

VIII. TWO-CHANNEL STRUCTURE

An interesting system where the coupling to voltage and dephasing probes strongly affect the transport properties is shown in Fig. 9. This system was investigated theoretically by Texier and Büttiker^{17,18} and recently realized experimentally by Oberholzer et al.³⁶. It consists of a three terminal quantum hall bar to which an additional probe is connected. The coherent setup without the probe is displayed in the inset of Fig. 9. The filling factor is tuned to two, such that the current is carried by two parallel edge states propagating along the boundary of the sample.

The two quantum point contacts QPC 1 and QPC 3 work as beam splitters with T_1 (R_1) and T_3 (R_3) the transmission (reflection) probabilities respectively. Both quantum point contacts are completely open for the outer channel. We consider the case of zero temperature and a voltage is applied at terminal 1, while the terminals 2 and 3 are kept at ground.

In the original investigation the focus was on the cross-correlations between the currents in terminal 2 and 3. It was shown by Texier and Büttiker that the sign of the cross-correlations depends on whether a voltage or a dephasing probe is coupled to the system. In the case $T_3 = 0$, the inner channel leads to contact 2 and the outer to contact 3. Then for the coherent system the cross-correlations C_{23} vanish, a voltage probe introduces *positive* cross-correlations, and for a dephasing probe the correlations turn out to be *negative*. The positive cross-correlations have been measured recently by Oberholzer et al.³⁶.

It is interesting to understand these statistical effects on the level of the generating function. The generating function especially enlightens the difference between voltage and dephasing probes, which is present only in the case of more than one transport channel if scattering is energy independent.

We start again with the coherent system without the probe. From Eq. (6) the generating function S_0 reads:

$$S_0 = N \ln [e^{i(\lambda_3 - \lambda_1)} (1 - T_1 + T_1 T_3 e^{i(\lambda_3 - \lambda_1)} + T_1 R_3 e^{i(\lambda_2 - \lambda_1)})] \quad (44)$$

The factor $e^{i(\lambda_3 - \lambda_1)}$ stands for the outer channel, where particles are transmitted from 1 to 3 with probability one, it represents a noiseless contribution to the current into terminal 3. The factor in the parentheses represents the inner channel, where an infalling particle is either reflected at beam splitter QPC 1 or transmitted into terminal 2 with probability $T_1 R_3$ or into 3 with probability $T_1 T_3$.

For $T_3 = 0$, the inner and outer channel lead into different contacts 2 and 3. Since in the absence of interchannel scattering the two modes are uncorrelated, the cross-correlations vanish, $C_{23} = 0$. When T_3 is greater than zero, the cross-correlations are negative, $C_{23} = -\frac{e^3 V}{h} T_1^2 T_3 R_3$, because QPC 3 acts as a beam splitter

for the inner mode (but the inner and outer channel are still uncorrelated).

We then consider an additional probe perfectly coupled to the system, see Fig. 9. To keep the discussion simple, we concentrate on the case $T_3 = 0$. The unconstrained function H_0 can be written in terms of independent one-particle scattering processes

$$H_0 = \ln \left[e^{i(\lambda_p - \lambda_1)} (1 - T_1 + T_1 e^{i(\lambda_p - \lambda_1)}) \times (1 - n_p + n_p e^{i(\lambda_2 - \lambda_p)}) (1 - n_p + n_p e^{i(\lambda_3 - \lambda_p)}) \right] \quad (45)$$

The first two factors correspond to the two transport modes emerging from terminal 1, and the rest describes the inner and outer channel from p to 2 or 3 respectively.

A. Voltage probe

In the presence of a voltage probe, n_p is an equilibrium Fermi function, and the potential V_p fluctuates in order to maintain zero net current flow into the probe. The formalism to obtain the FCS is presented in section VB. Because the current is transported by two modes, the argument of the logarithm in Eq. (45) is quadratic in n_p , but the energy integrated function \tilde{S}_V at zero temperature, Eq. (31) is still linear in V_p . The saddle point equations, Eq. (30) are easily solved, and the cumulant generating function is

$$S_V = N \ln \left[e^{i \frac{\lambda_2 + \lambda_3}{2}} \left(1 + T_1 (e^{i \frac{\lambda_2 + \lambda_3}{2}} - 1) \right) \right]. \quad (46)$$

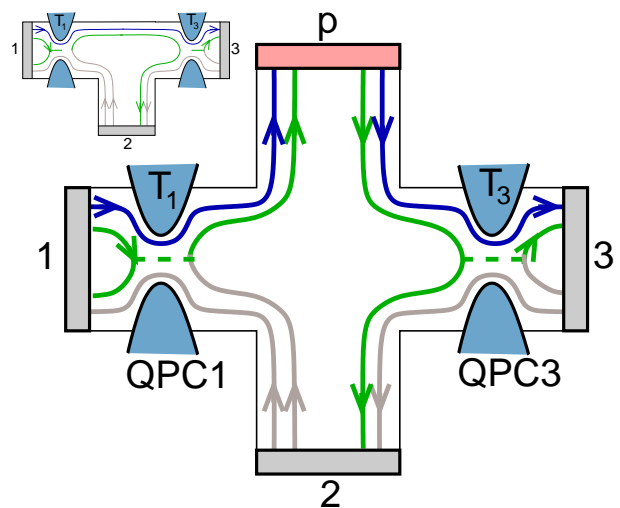


FIG. 9: (color online) Beam splitter with a probe: a three terminal quantum hall bar at filling factor 2 and one voltage/dephasing probe. The two quantum point contacts QPC 1 and QPC 3 are open for the outer transport channel. A voltage is applied on terminal 1, thus the channels shaded in (light) grey are effectively empty and do not matter. The inset shows the setup for the case when the connection to the probe is closed, i.e. when there is no probe connected to the beam splitter.

The first factor represents a noiseless stream from 1 to p which is divided into two noiseless streams in the two outgoing channels from p leading into contacts 2 and 3. The part inside the parentheses describes the inner channel. Passing through QPC 1 the incident stream at the probe is noisy and it is again equally divided into the outgoing channels.

Both outgoing channels are fully filled up to the energy $eV_p = eV_p(t)$. This creates a perfect correlation between the currents in 2 and 3, $I_2(t) = I_3(t)$, and is the reason for the positive cross-correlations given by $C_{23} = \frac{e^3 V R_1 T_1}{h}$. Technically the positive sign can be seen in the generating function Eq. (46), where the counting fields λ_2 and λ_3 appear only as a sum in the exponent. For a finite transmission T_3 the inner edge is split at the QPC 3, and the negative cross-correlations of this splitting compete¹⁷ with the positive correlations induced by the potential fluctuations at contact p .

The voltage probe thus acts as a noise divider³⁶, because both currents in 2 and 3 show fluctuations, in contrast to the coherent system where only the inner channel leading to contact 2 was noisy. As a consequence of current conservation, the noise of the current incident at the probe -created by the beam splitter QPC 1- equals the sum of current correlations emerging from the probe: $\frac{e^3 V}{h} R_1 T_1 = C_{22} + C_{33} + 2C_{23}$. Note that both auto- and cross-correlations vanish for $T_1 = 0$ separately.

The counting fields λ_2 and λ_3 appear with a factor $1/2$ in Eq. (46). We emphasize that the factor $1/2$ does not mean that the voltage probe emits half particles with charge $e/2$. The generating function only makes sense in the long time limit when many charges are emitted. Therefore, the factor $1/2$ simply describes the equal partition of the incident charges into two outgoing channels.

B. Dephasing probe

If instead of a voltage probe, a dephasing probe is coupled to the system, the cross-correlations are manifestly negative. The argument of the function H_0 , Eq. (45) is quadratic in the occupation number n_p , therefore, the saddle point equations, Eq. (20) are nonlinear. For the case $T_1 = 0$, when only the outer fully filled channel is transported to the probe, the saddle point equations are solved by $n_p^0 = 1/2$ and $\lambda_p^0 = (\lambda_2 + \lambda_3)/2$. The resulting generating function is

$$S_{T_1=0} = N \ln \left[\frac{1}{4} (e^{i\frac{\lambda_2}{2}} + e^{i\frac{\lambda_3}{2}})^2 \right] \quad (47)$$

Again the counting fields λ_2 and λ_3 appear with a factor $1/2$ displaying equal partition of the incident charges into the outgoing channels. In contrast to the voltage probe, the occupation of the channels going out from the dephasing probe is non-unity. This leads to noise in each of the two outgoing channels, despite the fact that the incoming current for $T_1 = 0$ is noiseless. As a consequence

of current conservation $0 = C_{22} + C_{33} + 2C_{23}$ the cross-correlations are negative: with $C_{23} = -\frac{e^3 V}{8h} = -C_{22} = -C_{33}$.

We have not been able to find analytically the exact constraint cumulant generating function for arbitrary T_1 . By expansion in the counting fields λ_2 and λ_3 the saddle point equations can be solved separately for each order in the counting fields and the solutions are found cumulant by cumulant. Another method is the expansion in small T_1 which leads to the constraint generating function to second order in T_1

$$S = S_{T_1=0} - \frac{N}{4} T_1 \left(e^{\frac{i}{2}(3\lambda_2 + \lambda_3)T_1} + e^{\frac{i}{2}(\lambda_2 + 3\lambda_3)T_1} + 2(2 + T_1) - 4e^{i\frac{\lambda_2 + \lambda_3}{2}T_1} (1 + T_1) \right) + \mathcal{O}(T_1^3) \quad (48)$$

The cumulants up to second order obtained by this generating functions are exact, because they are of second order in $T_1 = 1 - R_1$. The cross-correlations are always negative and given by $C_{23} = -\frac{e^3 V R_1^2}{8h}$, and the auto-correlations are $C_{22} = C_{33} = \frac{e^3 V R_1}{8h} (4 - 3R_1)$. The noise incident on the probe is $\frac{e^3 V}{h} R_1 (1 - R_1) = C_{22} + C_{33} + 2C_{23}$. Note that the incident noise is maximal for $R_1 = 1/2$, while the noise in terminal 2 and 3 has its maximum at $R_1 = 3/4$, and the cross-correlations are monotonously decreasing with R_1^2 .

IX. COMPARISON TO OTHER MODELS

It is interesting to compare our approach to closely related work. An important subject is phenomenological models of dephasing in chaotic cavities. Polianski and Brouwer¹³ investigated general time-dependent scattering in a chaotic dot, using a model where the dot is connected to a short stub with a fluctuating potential. Although the fluctuating potential leads to dephasing, it also creates noise which is an undesired feature for modeling pure dephasing. To overcome this problem Beenakker and Michaelis recently developed a stub model⁴⁶ with a long stub in which the dynamics was chaotic, i.e. in fact representing the stub as a second chaotic cavity. In the limit of a long dwell time of the stub they found that the additional noise created by the fluctuating potential in the stub was negligible compared to the regular shot noise.

Beenakker and Michaelis compared their model to a dephasing probe model with a static distribution function of the probe, chosen to yield zero average current into the probe. In such a dephasing probe model, the low frequency probe current in each measurement is not zero. Importantly, in our work we instead consider a probe model where the distribution function fluctuates in time as a response to the injected charge. The low frequency current is thus conserved in each measurement and intrinsically no additional noise is created. Consequently, our probe model has both the desired features of

a pure dephasing model, it does not introduce any additional noise and it conserves charge, or equivalently the low frequency current. It is at the present not clear to us whether an extension of the model of Ref. 46 to the FCS would yield the same result as our dephasing probe model in the corresponding parameter (many modes, weak coupling) limit.

In another recent work⁴⁵ San-Jose and Prada developed a method for investigating the effects of a charge conserving probe on the full counting statistics of coherent mesoscopic conductors with energy independent scattering. They consider a set of localized wave packets -“scattering events”- incident on the conductor during a time step $\Delta t = h/eV$. In the absence of probes, scattering events at different time steps are independent, and the Levitov-Lesovik result⁵, our Eq. (6), is recovered. Introducing probes connected to the conductor, scattering at different time steps becomes correlated: the number of charges injected into the probe at one time step determines the number of charges emitted from the probe in the next step (or next few steps). The full counting statistics is obtained in a way qualitatively similar to exclusion statistics models¹⁶. In contrast to the standard exclusion models the probabilities in the scheme of Ref. 45 are multi-particle scattering probabilities.

In the model of Ref. 45 all processes happen within the timescale Δt . The excess (deficit) charge in the probe is at most a few electrons. There is no separation of time-scales. This is clearly different in construction from our model where the probes contain a large number of electronic states and consequently respond to injected charges only on the timescale $\tau_d \gg \Delta t \equiv \tau_s$. Nevertheless, in the long time limit, we find that the FCS for an arbitrary mesoscopic conductor connected to a single mode probe is given by our Eq. (26), which holds both for dephasing and voltage probes.

In the case with multi-mode probes we have not found any general relation between the method of Prada and San Jose and our method. It should however be noted that for a number of simple examples investigated, we find that the method of Ref. 45 and our voltage probe (but not the dephasing probe) approach give the same long time transport statistics.

A third related work is by Jakobs, Meden, Schoeller and Enss about phase averaging versus dephasing in a ballistic, one-dimensional, three barrier setup¹⁹. They calculate the conductance as a function of temperature. Finite temperature leads to phase averaging due to the energy dependence of the phase picked up in scattering processes with multiple loops between the barriers. They find that the phase averaged conductance is $G \sim \sqrt{G_1 G_2 G_3}$ in the limit of small conductances G_i of the individual barriers.

This is different from the result obtained by summing up the classical probabilities for the scattering paths through the system. Clearly, this latter result is also obtained by coupling each of the inter-barrier regions to a dephasing probe.¹ The different results can, along the

same line as at the end of section VII, be explained in terms of the different effect of phase averaging and dephasing probes on interfering scattering paths that pass the two probes in different order. A detailed discussion of this is presented in appendix E.

X. CONCLUSION

In this work we have developed a theory of electron statistical transport for conductors with voltage and dephasing probes. Using a stochastic path integral approach we have formulated generating functions which determine conductance, noise and all higher order current cumulants. The extension of the discussion of probe models for current and noise to the level of full counting statistics makes it possible to compare the different models with each other on the level of the generating functions. The validity of this approach rests on the fact that probes respond to a change in their charge state with a certain delay time similar to a real voltmeter. Therefore, current conservation at these probes is not instantaneous: only the low frequency current cumulants into the probe vanish.

We find that for one single mode probe the generating functions for a conductor attached to either a dephasing or a voltage probe are identical. They are also equivalent to the phase average of the coherent generating function over an appropriate phase distribution, given by the phase distribution of a chaotic cavity. We emphasize that these probes are connected to the conductor in the same way: it is only the “boundary” condition at the probe which differs. These boundary conditions lead to an equilibrium Fermi distribution for the voltage probe, a non-equilibrium distribution for the dephasing probe and leads to coherent reflection in the case of a phase probe. In the phase averaging probe used here we average over a very specific phase which is external to the original coherent conductor. It is important that these basic facts are kept in mind when assessing the finding reported here that all three probes are in the single channel limit equivalent.

For more than one probe, (or a probe with two quantum channels) however, the equivalence does not hold. For the phase averaging procedure used here, certain interference terms can survive. Thus phase averaging and dephasing probes give different results. This is reminiscent to the well known fact that in mesoscopic conductors weak localization survives phase averaging but dephasing suppresses weak localization. Similarly, phase averaging probes leave interferences between certain paths unaffected but dephasing probes destroy the interference between these paths.

In the case of multiple or multichannel probes it is not only the equivalence between phase averaging probes and dephasing probes which is lost but also the equivalence between dephasing and voltage probes. The different electron distributions in dephasing and voltage probes

become important and lead to different transport statistics. A spectacular emergence of this is the opposite sign of the current cross-correlations caused by either a voltage or a dephasing probe coupled to a conductor with two channels.

The full counting statistics of conductors in the presence of dephasing or voltage probes provide a deeper understanding of the physics of these probe models and will hopefully be a useful point of reference for future investigations. Many additional questions are of interest, for example how the probes affect the frequency dependent cumulants, or the connection between the semiclassical stochastic path integral and a full quantum approach or simply an investigation of the limit of large numbers of probes connected to a mesoscopic conductor.

Acknowledgement

This work was supported by the Swiss NSF, the Swiss National Center of Competence in Research MaNEP, the European Marie Curie MCTR-CT-2003-504574 and the Swedish VR. One of us (MB) likes to acknowledge the hospitality of the Aspen Center of Physics where part of this work was performed.

APPENDIX A: DERIVATION OF THE STOCHASTIC PATH INTEGRAL

The FCS for a conductor with M terminals connected to a dephasing probe can be derived in terms of a stochastic path integral. Since the charge on the dephasing probe is conserved for each energy interval dE and the occupation function $n_p(E, t)$ fluctuates independently in each interval, the distribution of charge transferred through the whole conductor is independent in each energy interval. Therefore, in this section we consider the charge transported in a small energy interval dE .

First, an intermediate time interval Δt is considered with $\tau_s \ll \Delta t \ll \tau_d$. We recall that $\tau_s^{-1} = eV/h$ is the rate at which carriers injected into the conductor and τ_d^{-1} is the much slower relaxation rate of distribution functions. The inequality $\Delta t \ll \tau_d$ implies that the charge transfer during time Δt only results in a marginal change of the charge in the terminals 1, 2, ... M as well as in the probe. The inequality $\tau_s \ll \Delta t$, on the other hand, leads to that the FCS during Δt is given by the Levitov-Lesovik formula, Eq. (7), with the energy integral replaced by the factor dE . To extend the FCS to longer times we write all the charges transported during the time interval as the difference between the charges in the terminals before and after the transfer, $\mathbf{Q}(t + \Delta t) - \mathbf{Q}(t) \equiv \mathbf{Q}_1 - \mathbf{Q}_0$, where $\mathbf{Q}(t) = (Q_1(t), \dots, Q_M(t), Q_p(t))$. We then make use of the composition property of the probabilities

$$P(\mathbf{Q}_2 - \mathbf{Q}_0) = \int d\mathbf{Q}_1 P(\mathbf{Q}_2 - \mathbf{Q}_1) P(\mathbf{Q}_1 - \mathbf{Q}_0), \quad (\text{A1})$$

where we use the notation $\int d\mathbf{Q} = \int dQ_1 \dots dQ_M dQ_p$. The probability to transfer $\mathbf{Q}_2 - \mathbf{Q}_0$ charges during the time interval $2\Delta t$ is obtained by multiplying the transfer probabilities in each interval Δt of $\mathbf{Q}_2 - \mathbf{Q}_1$ and $\mathbf{Q}_1 - \mathbf{Q}_0$ charges respectively, and integrating over all possible values of \mathbf{Q}_1 .

Extending this to the entire measurement time τ one has $P(\mathbf{Q}_k - \mathbf{Q}_0) = P(\mathbf{Q}_k - \mathbf{Q}_{k-1}) \prod_{n=1}^{k-1} \int d\mathbf{Q}_n P(\mathbf{Q}_n - \mathbf{Q}_{n-1})$, where $k = \tau/\Delta t$. This can be written with the help of Eqs. (1) and (6) as

$$P(\mathbf{Q}_k - \mathbf{Q}_0) = \int d\Lambda_0 \prod_{n=1}^{k-1} \int d\mathbf{Q}_n \int d\Lambda_n \quad (\text{A2}) \\ \times \exp \left[\sum_{n=0}^{k-1} -i\Lambda_n \cdot (\mathbf{Q}_{n+1} - \mathbf{Q}_n) + \frac{dE\Delta t}{h} H_0(\mathbf{Q}_n, \Lambda_n) \right]$$

The condition $\Delta t \gg \tau_s$ represents the long time limit, when H_0 does not depend on time and consequently $\int_0^{\Delta t} H_0 = \Delta t H_0$. The function H_0 depends here formally on all charges transmitted into the different terminals. However, it contains explicitly only the charge on the probe via $Q_p = en_p(E)\tau_d dE/h$, because the distribution functions of the terminals 1 to M are externally determined, (compare Eq. (7)).

Since the charges \mathbf{Q} only change slightly during the time interval $\Delta t \ll \tau_d$ we can take the continuum limit, in which $\mathbf{Q}_{n+1} - \mathbf{Q}_n = \Delta t \dot{\mathbf{Q}}_n$ and the sum in the exponent in Eq. (A2) becomes an integral. We moreover introduce the standard path integral notation $\int \mathcal{D}\mathbf{Q} \int \mathcal{D}\Lambda = \int d\Lambda_0 \prod_{n=1}^{k-1} \int d\mathbf{Q}_n \int d\Lambda_n$. This gives

$$P(\mathbf{Q}_k - \mathbf{Q}_0) = \int \mathcal{D}\mathbf{Q} \mathcal{D}\Lambda \\ \times \exp \left(\int_0^\tau dt \left[-i\Lambda \cdot \dot{\mathbf{Q}} + \frac{dE}{h} H_0(Q_p, \Lambda) \right] \right) \quad (\text{A3})$$

Our interest is the number of charges transported into and out of the electronic reservoirs 1 to M , the absorbed charge $\mathbf{Q}^a \equiv (Q_1, \dots, Q_M)$. We can first integrate by parts the term in the exponent $\int_0^\tau dt \Lambda^a \cdot \dot{\mathbf{Q}}^a = -\int_0^\tau dt \dot{\Lambda}^a \cdot \mathbf{Q}^a + (\Lambda_k^a \cdot \mathbf{Q}_k^a - \Lambda_0^a \cdot \mathbf{Q}_0^a)$ and then functionally integrate over \mathbf{Q}^a to get $\delta(\dot{\Lambda}^a)$. This functional delta function just gives that $\Lambda^a = (\lambda_1, \dots, \lambda_M)$ are independent of time and the functional integrals over Λ^a are reduced to standard integrals. Then we have

$$P(\mathbf{Q}_k - \mathbf{Q}_0) = \int d\Lambda^a \exp(-i\Lambda^a \cdot (\mathbf{Q}_k^a - \mathbf{Q}_0^a)) \quad (\text{A4}) \\ \times \int \mathcal{D}Q_p \mathcal{D}\lambda_p \exp \left(\int_0^\tau dt \left[-i\lambda_p \dot{Q}_p + \frac{dE}{h} H_0(Q_p, \Lambda) \right] \right)$$

By choosing the boundary conditions so that $\lambda_p(t + \tau) = 0$ we consider the case where the charge Q_p is not detected, i.e. it is integrated over and we have $P(\mathbf{Q}_k - \mathbf{Q}_0) \rightarrow P(\mathbf{Q}_k^a - \mathbf{Q}_0^a)$. This gives the FCS for

the charge in the energy interval dE transported between the reservoirs 1 to M during the measurement time τ .

As a last step, we sum up the independent contributions from all the energy intervals. Making use of the relation $Q_p = en_p(E)\tau_d dE/h$, this leads to an energy integral in the exponent, and a path integral in the field $n_p(E, t)$, and we find the Eqs. (14) and (15) in section V A describing the generating function

$$\exp(S) = \int \mathcal{D}n_p \mathcal{D}\lambda_p \exp \tilde{S} \quad \text{with} \quad (\text{A5})$$

$$\tilde{S} = \frac{1}{h} \int_0^\tau dt \int dE [-i\tau_d \lambda_p \dot{n}_p + H_0]. \quad (\text{A6})$$

For the voltage probe on instead right from the outset considers the total energy integrated charge $Q_p = (e\tau_d/h) \int dE n_p(E)$ and correspondingly the energy integrated generating function $\int dE H_0$. Making use of the relation for an equilibrium distribution function $n_p(E)$

$$\dot{Q}_p = \frac{e\tau_d}{h} \int dE \frac{dn_p}{dV_p} \dot{V}_p = \frac{e\tau_d}{h} \dot{V}_p \int dE \frac{dn_p}{dV_p} = \frac{e^2 \tau_d}{h} \dot{V}_p \quad (\text{A7})$$

we directly arrive at Eq. (27).

APPENDIX B: SADDLE POINT CORRECTIONS

In section V A, the stochastic path integral Eq. (14) was evaluated in saddle point approximation. The function \tilde{S} is expanded around the saddle point, see Eq. (17). Taking into account the Gaussian fluctuations around the saddle point, the constraint generating function becomes $S = S^0 + \delta S$, where the upper index 0 stands here for the solution at the saddle point. As shown in the following, the corrections δS are of order τ_s/τ_d smaller than S^0 and can be neglected in the case $\tau_d \gg \tau_s$ considered here.

For simplicity we consider here energy independent scattering and a dephasing probe, other cases are treated analogously. In this case, the function $S = S^0 + \delta S$ can be evaluated for each energy interval independently or alternatively we can directly introduce a factor eV in place of the energy integral. We introduce the abbreviations $\lambda = \Delta\lambda_p$ and $n = \Delta n_p$ for the deviations away from the saddle point (λ_p^0, n_p^0) . Following standard path integral procedures for saddle point corrections⁵³, we insert the definition of \tilde{S} , Eq. (15) and discretizing time we find for the expansion around the saddle point, Eq. (17)

$$\begin{aligned} \tilde{S} &= \tilde{S}^0 + \frac{eV}{h} \sum_{k=1}^K [-i\tau_d \lambda_k (n_{k+1} - n_k) \quad (\text{B1}) \\ &+ \frac{dt}{2} (\lambda_k \ n_k) \begin{pmatrix} -A & iB \\ iB & C \end{pmatrix} \begin{pmatrix} \lambda_k \\ n_k \end{pmatrix} \Big], \end{aligned}$$

where the matrix elements $A = \left(\frac{\partial^2 H_0}{\partial \lambda_p^2} \right)$, $B = \left(\frac{\partial^2 H_0}{\partial \lambda_p \partial n_p} \right)$ and $C = \left(\frac{\partial^2 H_0}{\partial n_p^2} \right)$ contain second order derivatives of the

function H_0 evaluated at the saddle point. The upper bound of the sum is $K = \tau/dt$ and dt will be taken infinitesimal small.

In order to obtain a purely quadratic matrix form it is convenient to use the Fourier transforms $\lambda_k = \frac{1}{\sqrt{K}} \sum_{l=-K/2}^{K/2} e^{-\frac{2\pi i}{K} kl} \Lambda_l$ and $n_k = \frac{1}{\sqrt{K}} \sum_{l=-K/2}^{K/2} e^{-\frac{2\pi i}{K} kl} N_l$. One arrives at

$$\tilde{S} = \tilde{S}^0 - \frac{1}{2} \frac{eV}{h} \sum_{l>0} (\Lambda_l \ N_l \ \Lambda_{-l} \ N_{-l}) \Upsilon_l \begin{pmatrix} \Lambda_l \\ N_l \\ \Lambda_{-l} \\ N_{-l} \end{pmatrix} \quad (\text{B2})$$

where the matrix Υ_l has non-zero elements $\Upsilon_{13} = \Upsilon_{31} = A dt$, $\Upsilon_{24} = \Upsilon_{42} = -C dt$, $\Upsilon_{14} = \Upsilon_{41} = 2i\tau_d \left(e^{\frac{2\pi i l}{K}} - 1 \right) - iB dt$, $\Upsilon_{23} = \Upsilon_{32} = 2i\tau_d \left(e^{-\frac{2\pi i l}{K}} - 1 \right) - iB dt$. The resulting Gaussian integral $\int d\Lambda_l dN_l d\Lambda_{-l} dN_{-l} \exp(\tilde{S} - \tilde{S}^0)$ is proportional to $(\det \Upsilon_l)^{-1/2}$ with

$$\sqrt{\det \Upsilon_l} = \left| (B^2 - AC)(dt)^2 + 4\tau_d(\tau_d + Bdt) \sin^2 \frac{\pi l}{K} \right|. \quad (\text{B3})$$

In the limit $dt \rightarrow 0$ we can expand the sine since only small $l/K \ll 1$ contribute in the sum \sum_l in Eq. (B2). The term Bdt can be neglected and we arrive at the constraint generating function

$$S = \frac{eV\tau}{h} H_0(\lambda_p^0, n_p^0) - \sum_l \ln |\kappa^2 + x_l^2| + \text{const}, \quad (\text{B4})$$

where $\kappa^2 = B^2 - AC$ and $x_l = \frac{4\pi\tau_d l}{\tau}$. The first term is the solution S^0 at the saddle point which is already normalized, $S^0(\mathbf{\Lambda} = \mathbf{0}) = 0$. The second term represents the Gaussian corrections. We transform the sum into an integral $\sum_l \ln |\kappa^2 + x_l^2| \rightarrow \frac{\tau}{4\pi\tau_d} \int_0^\infty dx \ln |\kappa^2 + x^2|$. This contains a divergent contribution which stems from the missing normalization. To obtain the correct normalized function we take the derivative of δS with respect to the counting variables $\mathbf{\Lambda}$ in the terminals

$$\frac{d\delta S}{d\mathbf{\Lambda}} = -\frac{\tau}{4\pi\tau_d} \frac{d\kappa}{d\mathbf{\Lambda}} \int_0^\infty dx \frac{2\kappa}{\kappa^2 + x^2} = -\frac{\tau}{4\tau_d} \frac{d\kappa}{d\mathbf{\Lambda}} \quad (\text{B5})$$

We integrate again and find for the generating function

$$S = S^0 + \delta S = \frac{eV\tau}{h} \left(H_0(\lambda_p^0, n_p^0) - \frac{\tau_s}{4\tau_d} (\kappa(\mathbf{\Lambda}) - \kappa(\mathbf{0})) \right) \quad (\text{B6})$$

with the correct normalization $S(\mathbf{\Lambda} = \mathbf{0}) = 0$. The factor $\frac{\tau_s}{\tau_d} = \frac{h}{eV\tau_d}$ is just the ratio between the average time between two wave packets $\tau_s = h/eV$ and the much longer delay time of the probe τ_d , and thus the correction δS is small compared to the contribution of the saddle point S^0 .

APPENDIX C: PHASE AVERAGING AND FLUCTUATING PHASES

In section VII we compared the result of the dephasing probe with phase averaging of the generating function and found that the two approaches coincide for the case of a uniform phase distribution. We pointed out that such a phase averaging corresponds to an average over ensembles of a chaotic cavities, i.e. an average over static disorder. Here we would like to clarify that for the physical situation with a phase that fluctuates in time during the measurement process, an average of the fluctuating phase does in general not correspond to a phase average over the cumulant generating function.

For a phase that fluctuates in time, to find the correct averaging procedure it is necessary to compare the timescale of the phase fluctuations (say τ_d) with the measurement time τ . Let us take $P(Q)$ the probability that Q charges are transferred during the measurement. In a gedanken experiment, one would need to perform $m \gg 1$ measurements of the transferred charge to collect enough statistics in order to determine the FCS. Three different cases can then be distinguished.

i) $\tau_d \gg m\tau$. This corresponds to the situation that the phase is changing so slowly that it is possible perform m measurements without the phase changing. This means that all the cumulants, or equivalently the cumulant generating function, can be determined for a given phase φ . Repeating the experiment many times, for different phases, one can then obtain the phase averaged cumulant generating function $\langle S(\varphi) \rangle_\varphi$. This is thus equivalent to the average over static disorder.

ii) $\tau \ll \tau_d \ll m\tau$. In this case the phase is constant during a single measurement, however it varies from measurement to measurement. As a consequence, the charge statistics obtained by measuring a large number of times is the phase average of the probability distribution itself, $\langle P(Q, \varphi) \rangle_\varphi$, or equivalently the phase averaged moment generating function $\langle \exp[S(\varphi)] \rangle_\varphi$.

iii) $\tau_d \ll \tau$. For this situation the phase is fluctuating rapidly during a single measurement. The probability distribution giving the statistics outcome of a single measurement is independent on the phase, it is already given by the phase average $\langle P(Q, \varphi) \rangle_\varphi$. Performing a large number of measurements thus gives the same result as in ii).

It is important to note that the two averaged functions $\langle S \rangle_\varphi$ and $\langle e^S \rangle_\varphi$ coincide only to linear order in voltage, the average of the moment generating function leads to modulation contributions in the cumulants which are due to the modulation of conductance in time during the experiment and are of higher order in voltage^{25,27}.

APPENDIX D: PROOF OF EQUIVALENCE OF ONE-CHANNEL DEPHASING AND PHASE AVERAGING

Here we demonstrate the equivalence between phase averaging and the dephasing probe for a single mode probe connected to an arbitrary M -mode scatterer. We want to make use of the multi-particle probability expansion of the cumulant generating function in Eq. (8) and therefore consider the matrix $\mathcal{S}_{\{b\}}^{\{a\}}$. This matrix is formed by taking the intersecting matrix elements of the columns corresponding to the elements in $\{a\}$ and the rows corresponding to the elements in $\{b\}$ from the scattering matrix \mathcal{S} . For convenience of notation we use Eq. (41), the scattering matrix \mathcal{U} of the entire $M+1$ mode system. It is then possible to write

$$\mathcal{S}_{\{b\}}^{\{a\}} = \mathcal{U}_{\{b\}}^{\{a\}} + \mathcal{U}_{\{\phi\}}^{\{a\}} \frac{e^{i\varphi}}{1 - \mathcal{U}_{\{\phi\}}^{\{\phi\}} e^{i\varphi}} \mathcal{U}_{\{b\}}^{\{\phi\}} \quad (\text{D1})$$

Making use of the general determinant relation

$$\det \begin{pmatrix} V & W \\ X & Y \end{pmatrix} = \det(Y) \det(V - XY^{-1}W) \quad (\text{D2})$$

we can write

$$\det \left(\mathcal{S}_{\{b\}}^{\{a\}} \right) = \left[1 - \mathcal{U}_{\{\phi\}}^{\{\phi\}} e^{i\varphi} \right]^{-1} \times \det \begin{pmatrix} \mathcal{U}_{\{b\}}^{\{a\}} & \mathcal{U}_{\{b\}}^{\{\phi\}} \\ -e^{i\varphi} \mathcal{U}_{\{\phi\}}^{\{a\}} & 1 - \mathcal{U}_{\{\phi\}}^{\{\phi\}} e^{i\varphi} \end{pmatrix} \quad (\text{D3})$$

Developing this determinant by the last row one obtains finally

$$\det \left(\mathcal{S}_{\{b\}}^{\{a\}} \right) = \left[1 - \mathcal{U}_{\{\phi\}}^{\{\phi\}} e^{i\varphi} \right]^{-1} \times \left[\det \left(\mathcal{U}_{\{b\}}^{\{a\}} \right) - e^{i\varphi} \det \left(\mathcal{U}_{\{b,\phi\}}^{\{a,\phi\}} \right) \right] \quad (\text{D4})$$

Taking the modulus square of this determinant and inserting it into the expression for the cumulant generating function expanded in terms of multi-particle scattering probabilities, Eq. (7), we arrive after some algebra at

$$H_0(\varphi) = \ln [\mathcal{A} + \mathcal{B}_1 e^{i\varphi} + \mathcal{B}_2 e^{-i\varphi}] - \ln [1 - \mathcal{U}_{\{\phi\}}^{\{\phi\}} e^{i\varphi}] \quad (\text{D5})$$

Here \mathcal{A} is defined in Eq. (26) above and

$$\begin{aligned} \mathcal{B}_1 &= \det \left[1 + \bar{n}_1 (\bar{\lambda}_1^\dagger \tilde{\mathcal{U}}^\dagger \bar{\lambda}_1 \mathcal{U} - 1) \right] \\ \mathcal{B}_2 &= \det \left[1 + \bar{n}_1 (\bar{\lambda}_1^\dagger \mathcal{U}^\dagger \bar{\lambda}_1 \tilde{\mathcal{U}} - 1) \right] \end{aligned} \quad (\text{D6})$$

with \bar{n}_1 and $\bar{\lambda}_1$ defined in Eq. (22). We also introduced the matrix

$$\tilde{\mathcal{U}} = \begin{pmatrix} \mathcal{S}_{00} & 0 \\ 0 & 1 \end{pmatrix} \quad (\text{D7})$$

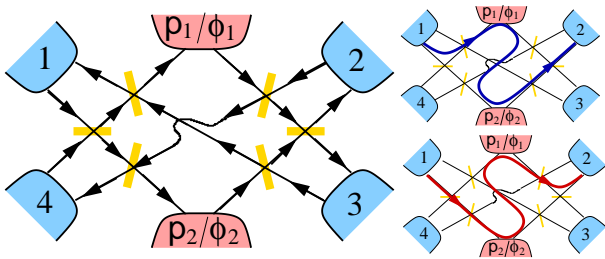


FIG. 10: A four terminal geometry with two probes attached. The direction of transport channels is indicated by arrows, the intersections marked with yellow bars represent beam splitters. Interference between paths passing through the probes in different order as shown on the right is destroyed by dephasing probes, but not by phase averaging.

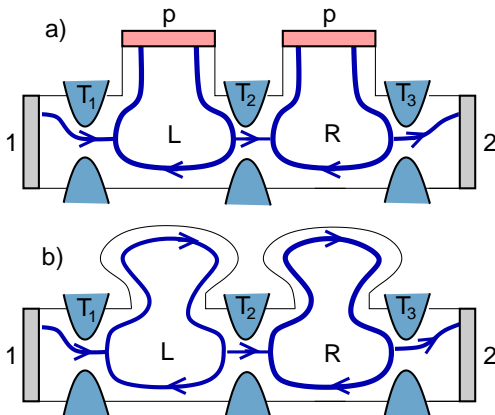


FIG. 11: Three barrier setup with two dephasing probes (a) or two elastic scatterer (b). While the probes destroy the phase memory in each loop individually, the elastic scatterer (phase averaging) allow coherent multiple loops.

Performing the phase average in Eq. (43), we arrive at the cumulant generating function

$$\langle S \rangle_\varphi = \ln \left[\frac{1}{2} \left(\mathcal{A} + \sqrt{\mathcal{A}^2 - 4\mathcal{B}_1\mathcal{B}_2} \right) \right] \quad (\text{D8})$$

It is then a lengthy but straightforward exercise in determinant algebra to show that

$$\mathcal{B}_1\mathcal{B}_2 = \mathcal{B} \quad (\text{D9})$$

where \mathcal{B} is defined in Eq. (26). This concludes the proof that the result for phase averaging, Eq. (D8) is identi-

cal to the result with a dephasing probe, Eq. (26), for a single mode probe connected to an arbitrary mesoscopic scatterer.

APPENDIX E: TWO PROBES

The agreement between the dephasing probe model and phase averaging found for a single mode probe does not hold anymore for the case of several probes or of probes with more than one transport channel. Differences occur already on the level of conductance. A qualitative understanding of the difference between phase averaging and dephasing probes can be obtained for the simplest possible case with two single mode probes. The difference arises due to scattering trajectories that visit the two probes in different order, but each probe the same number of times. These paths give rise to an interference term in the conductance that survives phase averaging but is destroyed by the dephasing probes.

The most elementary paths going from say terminal α to β , via the probes p_1 and p_2 are then $\alpha \rightarrow p_1 \rightarrow p_2 \rightarrow \beta$ and $\alpha \rightarrow p_2 \rightarrow p_1 \rightarrow \beta$. An example of a geometry where such elementary paths are possible is shown in Fig. 10. It contains two dephasing probes p_1 and p_2 or two elastic scatterer ϕ_1 and ϕ_2 . Transport is unidirectional, and six reflection-less beam splitters divide the currents in the setup as is indicated by arrows in the figure. The crossing in the center of the structure means that the beams are not divided but pass one on top of the other.

The geometry in Fig. 10 is rather complex. A simpler three-barrier geometry where phase averaging and dephasing give different results were recently proposed in Ref. 19 and discussed in section IX, a schematic picture is shown in Fig. 11. Dephasing probes or elastic scatterer are connected to the regions between the barriers. The most elementary paths responsible for the difference between phase averaging and dephasing probes in this geometry are $\alpha \rightarrow p_1 \rightarrow p_2 \rightarrow p_1 \rightarrow p_2 \rightarrow \beta$ and $\alpha \rightarrow p_1 \rightarrow p_1 \rightarrow p_2 \rightarrow p_2 \rightarrow \beta$, with $\alpha = 1$ and $\beta = 2$ in Fig. 11. These paths are thus more complicated than the elementary paths in the geometry in Fig. 10. We must leave it as a further challenge to find additional simple geometries for which dephasing and phase averaging leads to different results.

¹ M. Büttiker, IBM J. Res. Develop., **32**, 63-75 (1988).

² M. J. M. de Jong and C. W. J. Beenakker, Physica A **230**, 219 (1996).

³ L. S. Levitov, H. Lee, and G. B. Lesovik, J. Math. Phys. **37**, 4845 (1996).

⁴ S. Pilgram, P. Samuelsson, H. Förster, and M. Büttiker,

Phys. Rev. Lett. **97**, 066801 (2006).

⁵ L. S. Levitov and G. Lesovik, JETP Lett. **58**, 230 (1993).

⁶ *Quantum Noise in Mesoscopic Physics*, edited by Yu. V. Nazarov (Kluwer, Dordrecht, 2003).

⁷ M. Büttiker, Phys. Rev. B **38**, 9375, (1988).

⁸ T. Ando, Surface Science **361/362**, 267 (1996); Physica E

- 20, 24 (2003).
- ⁹ A. A. Clerk and A. D. Stone, Phys. Rev. B **69**, 245303 (2004).
 - ¹⁰ M. Moskalets and M. Büttiker, Phys. Rev. B **64**, 201305 (2001).
 - ¹¹ V. S.-W. Chung, M. Moskalets, and P. Samuelsson, (unpublished).
 - ¹² C. W. J. Beenakker, Rev. Mod. Phys. **69**, 000731 (1997).
 - ¹³ M. L. Polianski and P. Brouwer, J. Phys. A: Math. Gen. **36**, 3215 (2003).
 - ¹⁴ C. W. J. Beenakker and M. Büttiker, Phys. Rev. B **46**, 1889 (1992).
 - ¹⁵ S. A. van Langen and M. Büttiker, Phys. Rev. B **56**, 1680 (1997); Ya. M. Blanter, H. Schomerus, and C. W. J. Beenakker, Physica E **11**, 1 (2001); K. E. Nagaev, P. Samuelsson, and S. Pilgram, Phys. Rev. B **66**, 195318 (2002).
 - ¹⁶ P.-E. Roche, B. Derrida, and B. Doucot, Eur. Phys. J. B **43**, 529 (2005).
 - ¹⁷ C. Texier and M. Büttiker, Phys. Rev. B **62**, 7454 (2000).
 - ¹⁸ M. Büttiker, in *Quantum Noise in Mesoscopic Physics*, edited by Yu. Nazarov (Kluwer, Dordrecht, 2003). p.3
 - ¹⁹ S. Jakobs, V. Meden, H. Schoeller, and T. Enss, cond-mat/0606486 (unpublished).
 - ²⁰ G. Seelig and M. Büttiker, Phys. Rev. B **64**, 245313 (2001).
 - ²¹ G. Seelig, S. Pilgram, A. N. Jordan, and M. Büttiker, Phys. Rev. B **68**, 161310 (2003).
 - ²² K. Le Hur, Phys. Rev. B **65** 233314 (2002).
 - ²³ K. Le Hur, cond-mat/0606387 (unpublished).
 - ²⁴ Y. Ji, Y. Chung, D. Sprinzak, M. Heiblum, D. Mahalu, and H. Shtrikman, Nature **422**, 415 (2003).
 - ²⁵ F. Marquardt and C. Bruder, Phys. Rev. Lett. **92**, 56805 (2004); Phys. Rev. B **70**, 125305 (2004).
 - ²⁶ F. Marquardt, Europhys. Lett. **72**, 788 (2005).
 - ²⁷ H. Förster, S. Pilgram, and M. Büttiker, Phys. Rev. B **72**, 075301 (2005).
 - ²⁸ V. S.-W. Chung, P. Samuelsson, and M. Büttiker, Phys. Rev. B **72**, 125320 (2005).
 - ²⁹ E. V. Sukhorukov and V. V. Cheianov, cond-mat/0609288 (unpublished).
 - ³⁰ I. Neder, M. Heiblum, Y. Levinson, D. Mahalu, and V. Umansky, Phys. Rev. Lett. **96**, 016804 (2006).
 - ³¹ L. V. Litvin, H.-P. Tranitz, W. Wegscheider, and C. Strunk, cond-mat/0607758 (unpublished).
 - ³² S. Oberholzer, M. Henny, C. Strunk, C. Schönenberger, T. Heinzel, K. Ensslin, and M. Holland, Physica E **6**, 314 (2000).
 - ³³ M. Henny, S. Oberholzer, C. Strunk, T. Heinzel, K. Ensslin, M. Holland, and C. Schönenberger, Science **284**, 296 (1999); W. D. Oliver, et al. J. Kim, R. C. Liu, and Y. Yamamoto, Science **284**, 299 (1999).
 - ³⁴ S.-T. Wu and S.-K. Yip, Phys. Rev. B **72**, 153101 (2005); S.-T. Wu and S.-K. Yip, cond-mat/0603311 (unpublished).
 - ³⁵ V. S. Rychkov and M. Büttiker, Phys. Rev. Lett. **96**, 166806 (2006).
 - ³⁶ S. Oberholzer, E. Bieri, C. Schönenberger, M. Giovannini, and J. Faist, Phys. Rev. Lett. **96**, 046804 (2006).
 - ³⁷ M. Büttiker, Science **313**, 1587 (2006).
 - ³⁸ M. Büttiker, Phys. Rev. B **32**, 1846 (1985).
 - ³⁹ B. L. Altshuler, A. G. Aronov, and D. E. Khmelnitskii, J. Phys. C **15**, 7367 (1982).
 - ⁴⁰ S. Datta, Phys. Rev. B **40**, 5830 (1989); Nanotechnology **15**, 433 (2004).
 - ⁴¹ H. M. Pastawski, Phys. Rev. B **44**, 6329 (1991); Phys. Rev. B **46**, 4053 (1992); L. E. F. Foa Torres, H. M. Pastawski, and E. Medina, Europhys. Lett. **73**, 164 (2006).
 - ⁴² S. Pilgram, A. Jordan, E. V. Sukhorukov, and M. Büttiker, Phys. Rev. Lett. **90**, 206801 (2003); S. Pilgram, Phys. Rev. B **69**, 115315 (2004).
 - ⁴³ A. N. Jordan, E. V. Sukhorukov, and S. Pilgram, J. Math. Phys. **45**, 4386 (2004).
 - ⁴⁴ E. Prada, F. Taddei, and R. Fazio, Phys. Rev. B **72**, 125333 (2005).
 - ⁴⁵ P. San-Jose and E. Prada, Phys. Rev. B **74**, 045305 (2006).
 - ⁴⁶ C. W. J. Beenakker and B. Michaelis, J. Phys. A: Math. Gen. **38**, 10639 (2005).
 - ⁴⁷ A. D. Benoit, S. Washburn, C. P. Umbach, R. B. Laibowitz, and R. A. Webb, Phys. Rev. Lett. **57**, 1765 (1986).
 - ⁴⁸ K. L. Shepard, M. L. Roukes, and B. P. Van der Gaag, Phys. Rev. Lett. **68**, 2660 (1992); Phys. Rev. B **46**, 9648 (1992).
 - ⁴⁹ R. de Picciotto, H. L. Stormer, L. N. Pfeiffer, K. W. Baldwin, and K. W. West, Nature **411**, 51 (2001).
 - ⁵⁰ B. Gao, Y. F. Chen, M. S. Fuhrer, D. C. Glattli, and A. Bachtold, Phys. Rev. Lett. **95**, 196802 (2005).
 - ⁵¹ Ya. M. Blanter and M. Büttiker, Phys. Rep. **336**, 1 (2000).
 - ⁵² The generating function for networks of two-terminal conductors is derived in M. Kindermann, Yu. V. Nazarov, and C. W. J. Beenakker, Phys. Rev. B **79**, 035336 (2004).
 - ⁵³ J. Zinn-Justin, *Intégrale de chemin en mécanique quantique: Introduction* (CNRS Éditions, Paris, 2003).